Plasma Sources Science and Technology

PAPER

Electron impact excitation of allowed and forbidden transitions between fine-structure levels in Ti III

To cite this article: Yang Wang *et al* 2024 *Plasma Sources Sci. Technol.* **33** 115020

IOP Publishing Plasma Sources Science and Technology
Plasma Sources Sci. Technol. **33** (2024) 115020 (14pp) https://doi.org/10.1088/1361-6595/ad95b8

Electron impact excitation of allowed and forbidden transitions between fine-structure levels in Ti III

Yang Wang[1], Qiu-Yao Cao[1], Xi-Ming Zhu[1,*], Chun-Meng Du[1] and Klaus Bartschat[2]

[1] School of Physics, Harbin Institute of Technology, Harbin, Heilongjiang 150001, People's Republic of China
[2] Department of Physics and Astronomy, Drake University, Des Moines, IA 50311, United States of America

E-mail: simon.ximing.zhu@outlook.com

Received 18 June 2024, revised 23 October 2024
Accepted for publication 21 November 2024
Published 2 December 2024

Abstract

Introduction: We present an extensive theoretical investigation of the electron impact excitation of doubly-ionized titanium (Ti III) to meet the needs of spectral analysis and plasma modeling. OBJECTIVES: The main objective of this work is to extend the currently scarce database of both structure and collision data for Ti III. METHODS: The calculation was performed in the close-coupling approximation using the *B*-spline *R*-matrix method. The multi-configuration Hartree–Fock method in combination with *B*-spline configuration interaction expansions and the non-orthogonal orbitals technique is employed for accurate descriptions of the target wave functions and adequate accounts of the various interactions between the target states. Relativistic effects are treated at the semi-relativistic Breit-Pauli approximation level. RESULTS: The present close-coupling expansion includes 138 fine-structure levels of Ti III belonging to the $3d^2$, $4s^2$, $4s4p$, $3d4l$ ($l=0-3$), $3d5l$ ($l=0-3$), $3d6s$, and $3d6p$ configurations. Comprehensive sets of radiative and electron collisional data are reported for all of the possible transitions between the 138 fine-structure levels. Thermally averaged collision strengths are determined using a Maxwellian distribution for a wide range of temperatures from 10^2 K to 10^5 K. The accuracy of the calculated radiative parameters is validated by comparing with available values from the NIST database and previous literature. CONCLUSION: Given the lack of sufficient currently available experimental and theoretical data, the electron impact excitation cross sections of the Ti III fine-structure levels presented here are systematic, extensive, and internally consistent, thus making them suitable for many modeling applications.

Keywords: B-spline R-matrix, Ti III, electron impact excitation, excitation rate, fine-structure, cross section

1. Introduction

Accurate radiative and electron-collisional data for atoms and their ions are essential for the modeling and diagnostics of plasma sources with a reliable collisional-radiative (CR) model [1–5]. Titanium (Ti) and its ions are of particular significance for modeling non-equilibrium laboratory plasmas. Their spectra are frequently observed in plasma discharges, such as in the main cathodic ionizing products of a plasma propulsion device (μCAT) [6, 7], as well as in the self-sputtering phase of the HiPIMS discharge [8]. Therefore,

* Author to whom any correspondence should be addressed.

accurate and large atomic data sets, such as transition energies, oscillator strengths and collision cross sections, for Ti and its ions are required to develop a reliable CR model to extract detailed plasma parameters. However, compared to Ti I and Ti II, investigations on Ti III are scarce.

During the past few decades, experimental measurements and theoretical calculations of Ti III have mostly focused on its atomic structure and radiative parameters. Andersen *et al* [9, 10] measured the lifetimes of the $3d4p$ states for neutral and ionized Ti using the beam-foil technique. Roberts *et al* [11] experimentally determined absolute oscillator strengths for Ti I, Ti II, and Ti III transitions in the wavelength region from 244 nm to 350 nm using a wall-stabilized arc. Baudinet-Robinet *et al* [12] measured the lifetimes of several Ti III $3d4p$ levels from transitions observed between 70 nm and 190 nm.

On the theoretical side, considerable efforts have been made to generate accurate data of energy levels and radiative parameters for Ti III. Warner and Kirkpatrick [13] originally calculated the structure parameters of Ti III, including energy levels, oscillator strengths, and forbidden transition probabilities, in a single-configuration approximation. Biemont [14] presented calculations of oscillator strengths for ultraviolet lines from the $3d^n4s - 3d^n4p$ transitions ($n = 0-9$) in the doubly-ionized elements Sc III through Zn III. Beck [15] studied many-electron effects on electric quadrupole (E2) transition probabilities for $3d^2\ ^3F - 3d^2\ ^3P$ and $3d^2\ ^3F - 3d4s\ ^3D$ transitions using both analytic and numerical restricted Hartree–Fock wavefunctions. Biemont *et al* [16] performed calculations using three different theoretical methods, including relativistic Hartree–Fock (HFR), multi-configurational Dirac-Fock (MCDF), and SUPERSTRUCTURE (SST), respectively, for energy levels and transition probabilities involving the $3d^2$ configuration of the calcium iso-electronic sequence. The results of the three models were shown to be basically equivalent in the cases considered.

Next, Raassen and Uylings [17] employed the orthogonal operator method to calculate E1 , M1, and E2 transition probabilities in Ti III and T IV. Safronova *et al* [18] calculated energies and transition probabilities for the $3d^2$ states in Ca-like ions, including Ti III, with relativistic many-body perturbation theory (MBPT). Zhang *et al* [19] applied the weakest-bound-electron potential model (WBEPM) theory to calculate the transition probabilities and oscillator strengths for Ti III and Ti IV. El-Maaref *et al* [20] published a list of oscillator strengths, transition probabilities and lifetimes for Ti III generated with the CIV3 code. Relativistic effects and correlations up to the $6l$ orbitals were included in the calculations and shown to be important. Fivet *et al* [21] carried out a systematic study for M1 and E2 transition probabilities in doubly-ionized iron-peak elements including Ti III using two independent methods based on the HFR approach and the Thomas-Fermi–Dirac-Amaldi (TFDA) potential approximation. The results agreed with the earlier calculations [16, 17] to within 25%. Most recently, Maati *et al* [22] performed HFR and TFDA calculations to obtain a detailed list of energy levels and weighted oscillator strengths for Ti III. The results included states of 19 configurations: $3p^63d^2$, $3dnl$ ($n = 4-7$, $l = 0-3$), $3p^64s^2$, and $3p^64s4p$.

In comparison to the investigations on structure and radiative parameters of Ti III, studies of the dynamics of electron impact excitation processes are extremely scarce. To our knowledge, the only experimental excitation cross sections were measured by Popović *et al* [23] using the merged electron-ion beams energy-loss technique. They obtained absolute cross sections for the $3d^2\ ^3F - 3d4p\ ^3D,\ ^3F$ excitation of Ti III at energies ranging from 9 to 10 eV. Theoretical excitation cross sections for e−Ti III collisions are available on the IAEA ALADDIN database [24] for single-electron excitations from the ground configuration $3d^2$ to excited configurations $3d4l$ ($l = 0-3$), $3d5l$ ($l = 0-3$), $3d6s$, and $3d6p$.

Despite the longstanding interest in titanium from many researchers, systematic investigations on its doubly-charged ion Ti III are still lacking for both radiative parameters and electron impact excitation processes. The shortage of available data motivated us to carry out a detailed theoretical investigation of e−Ti III collisions. The purpose of the present work was to perform elaborate and extensive calculations for electron scattering from Ti III to provide comprehensive data sets of electron impact excitation cross sections and effective collision strengths, together with radiative transition data for a wide range of allowed and forbidden transitions in Ti III. The data sets provided are expected to meet the needs for analysis and interpretation of plasma modeling and diagnostics, as well as the titanium spectra.

The structure of Ti III can be considered as effectively a two-electron system above the $3s^23p^6$ core, which is supposed to be less complicated than that of other iron-peak elements. However, an accurate target description of Ti III is still very challenging due to the complexity of the open $3d$ sub-shell. The $3d$ valence electron experiences very strong interaction with the core electrons. This requires the inclusion of configurations with an open core, thereby resulting in large configuration expansions. On the other hand, different occupation numbers in the $3d$ sub-shell usually lead to a strong term dependence, which can be accounted for either by adding a number of specially designed pseudoorbitals to a set of orthogonal one-electron orbitals or by employing sets of term-dependent non-orthogonal orbitals. In practice, large configuration interaction (CI) expansions can quickly become computationally intractable in the case of open $3d$ sub-shell systems. Even though the term-dependent non-orthogonal orbitals approach also requires a significant number of non-orthogonal one-electron orbitals for high accuracy, it can be executed with computationally manageable CI expansions.

The present calculations were carried out in the close-coupling approximation using the sophisticated B-spline R-matrix (BSR) method [25]. The distinct feature of the BSR method is its ability to employ term-dependent non-orthogonal orbitals in the description of the target states. This allows us to optimize individual atomic wave functions independently and thereby generate a more accurate description of the target states with manageable CI expansions than what is usually possible when orthogonality restrictions are imposed. Over

the past decades, the BSR code (along with its fully relativistic extension, DBSR [26]) has been successfully applied to a number of targets [27]. More recent examples using the BSR code for electron impact excitation of iron-peak elements can be found in [28–31]. The BSR method generated very accurate target descriptions in all the above cases. In the present calculation, the close-coupling expansion included 138 fine-structure levels of Ti III belonging to terms of the ground $3d^2$ and excited $3d4l$ ($l=0-3$), $3d5l$ ($l=0-3$), $4s^2$, $4s4p$, $3d6s$, and $3d6p$ configurations. Relativistic effects were accounted for by the most important terms of the Breit-Pauli Hamiltonian.

This paper is organized as follows. The numerical approach applied to e−Ti III collisions is briefly summarized in section 2. References to more details are provided for interested readers. Section 3 presents and discusses the calculated results for the target energy levels, radiative parameters (transition probabilities, oscillator strengths, line strengths), as well as collisional parameters (excitation cross sections and effective collision strengths). The final set of radiative and collisional data includes 9453 transitions between the 138 fine-structure levels of Ti III. We also compare the present results with available calculations and, in rare cases, experimental data. Finally, a brief summary and conclusions are given in section 4.

2. Computational details

2.1. Structure calculations

The target states of Ti III in the present calculations were generated by combining the multi-configuration Hartree–Fock (MCHF) and the *B*-spline box-based CI code with with non-orthogonal orbitals [32]. Specifically, the structure of the multi-channel target expansion was chosen as

$$\begin{aligned}\Phi\left(3p^6nln'l',LSJ\right) = &\sum_{nl,LS}\left\{\phi\left(3p^63d\right)P\left(nl\right)\right\}^{LSJ}\\ &+\sum_{nl,LS}\left\{\phi\left(3p^64s\right)P\left(nl\right)\right\}^{LSJ}\\ &+\sum_{nl,LS}\left\{\phi\left(3p^64p\right)P\left(nl\right)\right\}^{LSJ}\\ &+a\varphi\left(3p^63d^2\right)^{LSJ}+b\varphi\left(3p^63d4s\right)^{LSJ}\\ &+c\varphi\left(3p^63d4p\right)^{LSJ}+d\varphi\left(3p^64s4p\right)^{LSJ}.\end{aligned} \tag{1}$$

Here $P(nl)$ denotes an orbital of the outer valence electron, while the ϕ and φ functions represent the CI expansions of the Ti IV and Ti III states, respectively. These expansions were generated in separate MCHF calculations for each state using the MCHF program [33]. The expansion (1) can be considered a model for the entire $3dnl$, $4snl$, and $4pnl$ Rydberg series in Ti III. The expansion can also provide a good approximation for the states with configurations $3d^2$, $3d4s$, $3d4p$, and $4s4p$. Alternatively, we may choose to employ separate CI expansions for these states by directly including relaxation and term-dependence effects via state-specific one-electron orbitals.

We performed a Hartree–Fock calculation to determine the $1s$, $2s$, and $2p$ orbitals of the inner frozen core $[1s^22s^22p^6]$ of the ground-state configuration $3s^23p^63d^2$, and the same core orbitals were used for all states considered in the present work. The core-valence correlation was accounted for through the CI expansions of the $3s^23p^63d$, $3s^23p^64s$ and $3s^23p^64p$ ionic states. These expansions included all single and double excitations from the $3s$ and $3p$ orbitals to the $4l$ and $5l$ ($l=0-3$) correlated orbitals. These orbitals were generated for each state separately. To keep the final expansions for the target states to a reasonable size, the CI expansions were initially restricted by dropping contributions with coefficients whose magnitude was less than the cut-off parameter of 0.01. Different terms of a configuration exhibited different convergence patterns and, therefore, required different cut-off parameters. Consequently, the final cut-off parameters were varied in the range from 0.008 to 0.012 for the different terms. The resulting CI expansions with sizes between 200 and 400 for each *LSJ* target state were manageable for the subsequent scattering calculation with currently available computational resources.

The unknown functions $P(nl)$ for the outer valence electron were expanded in a *B*-spline basis, and the corresponding equations were solved subject to the condition that the orbitals vanish at the boundary. The *R*-matrix boundary radius was set to $25\,a_0$, where $a_0 = 0.529\times10^{-10}\,\mathrm{m}$ is the Bohr radius. We employed 96 *B*-splines of order 8 to span this radial range using a semi-exponential knot grid. The *B*-spline coefficients for the valence electron orbitals $P(nl)$ and the perturbers were obtained by diagonalizing the semi-relativistic atomic Hamiltonian, which included all one-electron Breit-Pauli operators.

2.2. Scattering calculations

The scattering calculations were performed by employing an extended version of the BSR code [25]. The distinctive feature of the method is the use of *B*-splines as a universal basis to represent the scattering orbitals in the inner region of $r\leqslant a$. Hence, the *R*-matrix expansion in this region takes the form

$$\begin{aligned}&\Psi_k\left(x_1,\ldots,x_{N+1}\right)\\ &\quad=\mathcal{A}\sum_{ij}\bar{\Phi}_i\left(x_1,\ldots,x_N;\hat{\mathbf{r}}_{N+1}\sigma_{N+1}\right)r_{N+1}^{-1}B_j\left(r_{N+1}\right)a_{ijk}\\ &\quad+\sum_i\chi_i\left(x_1,\ldots,x_{N+1}\right)b_{ik}.\end{aligned} \tag{2}$$

Here the $\bar{\Phi}_i$ denote the channel functions constructed from the *N*-electron target states and the angular and spin coordinates of the projectile, while the splines $B_j(r)$ represent the radial part of the continuum orbitals. The χ_i are additional $(N+1)$-electron bound states, which are included to ensure completeness of the total trial wave function and to compensate for orthogonality constraints imposed on the continuum orbitals. Only limited orthogonality conditions on the continuum orbitals were needed (see below).

The $(N+1)$-electron Breit-Pauli Hamiltonian, with an additional Bloch term to ensure the hermiticity of the kinetic-energy operator, was diagonalized to determine the expansion coefficients a_{ijk} and b_{ik}. Relativistic effects in the scattering calculations were accounted for again through the one-electron terms of the Breit-Pauli Hamiltonian. We imposed only limited orthogonality conditions on the continuum orbitals with respect to the bound orbitals in the filled core shells $1s$, $2s$, $2p$, $3s$, and $3p$, but none on the spectroscopic excited orbitals or the correlation orbitals. Consequently, the second expansion in equation (2) was not needed in the present work. This helped to avoid pseudo-resonance structures in the final results.

The continuum orbitals in the internal region were expanded in the same B-spline basis as for the structure calculations described above. The present scattering model included 138 fine-structure levels of the Ti III $3d^2$, $4s^2$, $4s4p$, $3d4l$ ($l=0-3$), $3d5l$ ($l=0-3$), $3d6s$, and $3d6p$ configurations. This model will be labelled BSR-138 in the following discussion. The scattering calculations included up to 778 coupled scattering channels, and interaction matrices with dimensions of up to about 80 000 needed to be diagonalized for each partial wave. Partial-wave contributions up to $2J = 99$ were calculated explicitly, which was sufficient to obtain converged results for all optically forbidden transitions. For the optically allowed transitions, contributions from even higher partial waves were estimated by a top-up procedure based on the Coulomb-Bethe method or a geometric-series approximation. We employed a parallelized version of the BSR codes using MPI parallelization and the SCALAPACK libraries [34].

The scattering parameters were then found by matching the inner-region solutions at $r=a$ with the asymptotic solutions in the external region. A parallelized version of the STGF program [35] was employed in the external region to calculate the transition matrix elements, and from those the cross sections and collisions strengths using standard formulas [36]. In the resonance region for impact energies below the excitation energy of the highest level included in the close-coupling expansion, we used a fine energy step of 10^{-4} Ry to properly map out the relevant resonance structures. For energies above the highest excitation threshold included in the close-coupling expansion, the collision strengths vary smoothly, and hence we chose a coarser electron energy step of 10^{-2} Ry. We calculated collision strengths up to 10 Ry, which is sufficient to reach the asymptotic region for fitting to even higher incident energies. Altogether, over 10 000 energies for the colliding electron were considered.

The energy-dependent excitation cross section σ for an atomic transition can be derived from the collision strength Ω via

$$\sigma_{ij}(E) = \pi a_0^2 \frac{\Omega_{ij}(E)}{k_i^2 g_i}, \tag{3}$$

where i and j denote the initial and final states of the transition, respectively. Furthermore, k_i is the wave number of the colliding electron incident on the target ion in state i, a_0 is the Bohr radius, and $g_i = (2J_i + 1)$ is the statistical weight of state i.

The effective collision strengths or excitation rate coefficients as a function of electron temperature T_e are needed for applications in plasma modeling and spectral analysis. Effective collision strengths $\Upsilon(T_e)$ were calculated by convolving the collision strengths Ω over a Maxwellian distribution for electron temperatures from 10^2 K to 10^5 K as

$$\Upsilon_{ij}(T_e) = \int_{E_{th}}^{\infty} \mathrm{d}\left(\frac{E}{kT_e}\right) \Omega_{ij}(E) \exp\left(-\frac{E-E_{\mathrm{th}}}{kT_e}\right). \tag{4}$$

where T_e is the electron temperature, k is the Boltzmann constant, and E_{th} is the transition energy for the $i \rightarrow j$ transition. If needed, the excitation rates can be obtained by

$$C_{ij}(T_e) = \frac{8.629 \times 10^{-6}}{g_i T_e^{1/2}} \Upsilon_{ij}(T_e) \exp\left(-\frac{E_{th}}{kT_e}\right). \tag{5}$$

3. Results and discussion

3.1. Excitation energies and radiative parameters

Table 1 lists the present BSR calculations of target excitation energies and lifetimes for the first 118 levels of Ti III. We also included the recommended excitation energies from the NIST Atomic Levels and Spectra database [37] in the table. The levels in the table are arranged in order of calculated energies. Each level is defined by an index given in the first column. This index will be referred to in the following discussion to denote a particular transition. The overall agreement between experiment and theory is satisfactory, with the deviations in the energy splitting being less than 0.12 eV for most states. The maximum discrepancy in the present model is about 0.54 eV for the excitation threshold of the doubly excited $4s4p$ $^3\mathrm{P^o}$ states, which is due to the very slow convergence of the CI expansions for these levels.

The lifetimes of the excited levels given in table 1 were estimated from the calculated transition probabilities. The lowest 13 energy levels belong to the $3d^2$ and $3d4s$ configurations, which can only decay to lower levels via optically forbidden electric quadrupole (E2) and magnetic dipole (M1) transitions. Therefore, these 13 low-lying levels are all metastable states with their radiative lifetimes in the magnitude of seconds. The other levels can decay via allowed electric dipole (E1) transitions with their radiative lifetimes in the order of nanoseconds. A comparison of lifetimes for selected states of the $3d4p$ configuration is given in table 2 with the experimental measurements from Andersen *et al* [10] and Baudinet-Robinet *et al* [12]. The calculated lifetimes closely agree with the measurements of Andersen *et al*, except for the $^1\mathrm{D^o_2}$ state with a 26% deviation from experiment. The lifetimes measured by Baudinet-Robinet *et al* were mean values of the $3d4p$ $^3\mathrm{F^o}$ and $^3\mathrm{D^o}$ multiplets, and therefore have the same values for all levels in each multiplet. The present results for the $^3\mathrm{F^o}$ levels are in excellent agreement with experiment. A 34% deviation is seen for the $^3\mathrm{D^o}$ levels, where the reported values of the two experiments also differ from each other by about 18%. The present results still agree with the measurements of Andersen *et al* within the stated experimental uncertainties.

Table 1. Present calculated excitation level energies (in eV) and lifetimes (in ns) for Ti III.

Index	Conf.	Term	J	Energy	NIST [37]	Lifetime	Index	Conf.	Term	J	Energy	NIST [37]	Lifetime
1	$3d^2$	^{3}F	2	0.000	0.000	0.00×10^{00}	60	$3d5p$	^{3}P^o	0	18.608	18.476	3.69×10^{00}
2	$3d^2$	^{3}F	3	0.026	0.023	4.43×10^{12}	61	$3d5p$	^{1}P^o	1	18.635	18.524	2.15×10^{00}
3	$3d^2$	^{3}F	4	0.059	0.052	2.59×10^{12}	62	$3d5p$	^{3}P^o	2	18.637	18.507	3.76×10^{00}
4	$3d^2$	^{1}D	2	1.068	1.051	5.10×10^{10}	63	$3d5p$	^{1}F^o	3	18.661	18.555	2.41×10^{00}
5	$3d^2$	^{3}P	0	1.423	1.307	1.54×10^{10}	64	$4s4p$	^{1}P^o	1	19.440	19.491	4.20×10^{-1}
6	$3d^2$	^{3}P	1	1.432	1.315	1.53×10^{10}	65	$3d4f$	^{1}G^o	4	19.683	19.625	9.24×10^{-1}
7	$3d^2$	^{3}P	2	1.450	1.329	1.55×10^{10}	66	$3d4f$	^{3}F^o	2	19.728	19.656	6.93×10^{-1}
8	$3d^2$	^{1}G	4	1.879	1.785	6.49×10^{10}	67	$3d4f$	^{3}F^o	3	19.734	19.659	6.66×10^{-1}
9	$3d^2$	^{1}S	0	4.082	4.026	1.37×10^{8}	68	$3d4f$	^{3}F^o	4	19.748	19.675	6.92×10^{-1}
10	$3d4s$	^{3}D	1	4.644	4.719	1.68×10^{7}	69	$3d4f$	^{3}H^o	4	19.769	19.716	1.42×10^{00}
11	$3d4s$	^{3}D	2	4.664	4.736	1.68×10^{7}	70	$3d4f$	^{3}H^o	5	19.782	19.729	1.28×10^{00}
12	$3d4s$	^{3}D	3	4.697	4.764	1.66×10^{7}	71	$3d4f$	^{3}G^o	3	19.785	19.681	3.73×10^{-1}
13	$3d4s$	^{1}D	2	5.040	5.171	3.32×10^{7}	72	$3d4f$	^{3}G^o	4	19.808	19.697	3.95×10^{-1}
14	$3d4p$	^{1}D^o	2	9.342	9.323	1.76×10^{00}	73	$3d4f$	^{3}H^o	6	19.809	19.747	1.90×10^{00}
15	$3d4p$	^{3}D^o	1	9.523	9.547	1.10×10^{00}	74	$3d4f$	^{3}G^o	5	19.819	19.702	3.95×10^{-1}
16	$3d4p$	^{3}D^o	2	9.548	9.568	1.12×10^{00}	75	$3d4f$	^{1}D^o	2	19.823	19.729	6.19×10^{-1}
17	$3d4p$	^{3}D^o	3	9.583	9.599	1.12×10^{00}	76	$3d4f$	^{1}F^o	3	19.839	19.736	4.30×10^{-1}
18	$3d4p$	^{3}F^o	2	9.601	9.599	2.16×10^{00}	77	$3d4f$	^{3}D^o	1	19.873	19.762	4.91×10^{-1}
19	$3d4p$	^{3}F^o	3	9.641	9.639	2.12×10^{00}	78	$3d4f$	^{3}D^o	2	19.874	19.764	4.96×10^{-1}
20	$3d4p$	^{3}F^o	4	9.697	9.690	2.20×10^{00}	79	$3d4f$	^{3}D^o	3	19.882	19.773	4.85×10^{-1}
21	$3d4p$	^{3}P^o	0	10.119	10.036	1.21×10^{00}	80	$3d4f$	^{3}P^o	2	19.952	19.836	6.08×10^{-1}
22	$3d4p$	^{3}P^o	1	10.120	10.035	1.21×10^{00}	81	$3d4f$	^{3}P^o	1	19.966	19.850	6.12×10^{-1}
23	$3d4p$	^{3}P^o	2	10.135	10.046	1.21×10^{00}	82	$3d4f$	^{3}P^o	0	19.973	19.858	6.16×10^{-1}
24	$3d4p$	^{1}F^o	3	10.251	10.305	1.35×10^{00}	83	$3d4f$	^{1}H^o	5	19.980	19.844	3.82×10^{-1}
25	$3d4p$	^{1}P^o	1	10.470	10.389	1.37×10^{00}	84	$3d4f$	^{1}P^o	1	20.162	20.067	5.68×10^{-1}
26	$4s^2$	^{1}S	0	12.599	12.729	7.62×10^{1}	85	$3d5d$	^{1}F	3	20.825	20.795	3.11×10^{00}
27	$3d4d$	^{1}F	3	15.778	15.844	9.69×10^{-1}	86	$3d5d$	^{3}D	1	20.854	20.818	3.06×10^{00}
28	$3d4d$	^{3}D	1	15.878	15.924	9.53×10^{-1}	87	$3d5d$	^{3}D	2	20.867	20.833	3.06×10^{00}
29	$3d4d$	^{3}D	2	15.891	15.938	9.55×10^{-1}	88	$3d5d$	^{3}D	3	20.883	20.855	2.99×10^{00}
30	$3d4d$	^{3}D	3	15.909	15.955	9.60×10^{-1}	89	$3d5d$	^{3}G	3	20.888	20.848	2.94×10^{00}
31	$3d4d$	^{3}G	3	15.963	16.006	9.84×10^{-1}	90	$3d5d$	^{3}G	4	20.902	20.867	2.86×10^{00}
32	$3d4d$	^{3}G	4	15.983	16.025	9.90×10^{-1}	91	$3d5d$	^{1}P	1	20.923	20.872	3.41×10^{00}
33	$3d4d$	^{3}G	5	16.010	16.052	9.97×10^{-1}	92	$3d5d$	^{3}G	5	20.927	20.894	2.90×10^{00}
34	$3d4d$	^{1}P	1	16.022	16.025	1.07×10^{00}	93	$3d5d$	^{3}S	1	21.000	20.945	3.00×10^{00}
35	$3d4d$	^{3}S	1	16.230	16.210	1.01×10^{00}	94	$3d5d$	^{3}F	2	21.150	21.030	1.74×10^{00}
36	$4s4p$	^{3}P^o	0	16.485	17.018	7.45×10^{-1}	95	$3d6s$	^{3}D	1	21.155	21.062	1.50×10^{00}
37	$4s4p$	^{3}P^o	1	16.511	17.046	7.49×10^{-1}	96	$3d6s$	^{3}D	2	21.164	21.069	1.51×10^{00}
38	$4s4p$	^{3}P^o	2	16.565	17.105	7.56×10^{-1}	97	$3d5d$	^{3}F	3	21.167	21.049	1.75×10^{00}
39	$3d4d$	^{3}F	2	16.746	16.498	7.71×10^{-1}	98	$3d5d$	^{3}F	4	21.184	21.066	1.76×10^{00}
40	$3d4d$	^{3}F	3	16.761	16.516	7.74×10^{-1}	99	$3d6s$	^{3}D	3	21.198	21.109	1.50×10^{00}
41	$3d5s$	^{3}D	1	16.770	16.601	9.96×10^{-1}	100	$3d6s$	^{1}D	2	21.226	21.111	1.62×10^{00}
42	$3d4d$	^{3}F	4	16.780	16.536	7.78×10^{-1}	101	$3d5d$	^{3}P	0	21.283	21.149	2.24×10^{00}
43	$3d5s$	^{3}D	2	16.783	16.614	9.98×10^{-1}	102	$3d5d$	^{1}D	2	21.289	21.182	1.54×10^{00}
44	$3d5s$	^{3}D	3	16.813	16.648	9.97×10^{-1}	103	$3d5d$	^{3}P	1	21.336	21.159	1.64×10^{00}
45	$3d5s$	^{1}D	2	16.902	16.683	1.05×10^{00}	104	$3d5d$	^{1}G	4	21.336	21.219	1.95×10^{00}
46	$3d4d$	^{1}D	2	17.032	16.788	7.46×10^{-1}	105	$3d5d$	^{3}P	2	21.347	21.160	1.65×10^{00}
47	$3d4d$	^{3}P	0	17.106	16.805	9.05×10^{-1}	106	$3d5d$	^{1}S	0	21.539	21.372	2.01×10^{00}
48	$3d4d$	^{3}P	1	17.154	16.812	7.66×10^{-1}	107	$3d6p$	^{3}D^o	2	21.916		5.70×10^{00}
49	$3d4d$	^{1}G	4	17.154	16.904	9.60×10^{-1}	108	$3d6p$	^{3}D^o	1	21.929		4.87×10^{00}
50	$3d4d$	^{3}P	2	17.164	16.827	7.68×10^{-1}	109	$3d6p$	^{3}F^o	2	21.945		5.47×10^{00}
51	$3d4d$	^{1}S	0	17.662	17.360	1.05×10^{00}	110	$3d6p$	^{3}F^o	3	21.963		5.33×10^{00}
52	$3d5p$	^{1}D^o	2	18.356	18.252	3.43×10^{00}	111	$3d6p$	^{1}D^o	2	21.964		5.61×10^{00}
53	$3d5p$	^{3}D^o	1	18.397	18.295	2.49×10^{00}	112	$3d6p$	^{3}D^o	3	21.976		5.49×10^{00}
54	$3d5p$	^{3}D^o	2	18.419	18.319	2.55×10^{00}	113	$3d6p$	^{3}F^o	4	22.001		6.16×10^{00}
55	$3d5p$	^{3}D^o	3	18.441	18.342	2.50×10^{00}	114	$3d6p$	^{3}P^o	0	22.023		6.76×10^{00}
56	$3d5p$	^{3}F^o	2	18.445	18.341	3.53×10^{00}	115	$3d6p$	^{3}P^o	1	22.029		6.81×10^{00}
57	$3d5p$	^{3}F^o	3	18.466	18.363	3.54×10^{00}	116	$3d6p$	^{3}P^o	2	22.058		6.95×10^{00}
58	$3d5p$	^{3}F^o	4	18.501	18.401	3.55×10^{00}	117	$3d6p$	^{1}F^o	3	22.063		4.45×10^{00}
59	$3d5p$	^{3}P^o	1	18.592	18.471	1.89×10^{00}	118	$3d6p$	^{1}P^o	1	22.119		6.92×10^{00}

Table 2. Comparison of the present calculated lifetimes and experimental values for selected $3d4p$ states. The experimental values are from Andersen *et al* [10] and Baudinet-Robinet *et al* [12]. All values are in ns.

Index	Term	J	Present	Reference [10]	Reference [12]
14	^{1}D^o	2	1.76	2.4 ± 0.2	
15	^{3}D^o	1	1.10		1.7 ± 0.1
16	^{3}D^o	2	1.12		1.7 ± 0.1
17	^{3}D^o	3	1.12	1.4 ± 0.3	1.7 ± 0.1
19	^{3}F^o	3	2.12		2.1 ± 0.3
20	^{3}F^o	4	2.20	2.2 ± 0.3	2.1 ± 0.3
24	^{1}F^o	3	1.35	1.3 ± 0.2	
25	^{1}P^o	1	1.37	1.4 ± 0.2	

The spectral lines of optically allowed transitions usually receive most attention due to their importance in spectral analysis and plasma modeling. For Ti III, the ultraviolet lines between 200 nm and 300 nm are very important in many aspects of applications, such as studying the chemical imaging of various samples with plasma emission lines [38] and plasma modeling and diagnostics of plasma propulsion devices [6]. These emission lines are mostly related to transitions from the $3d4s$ to $3d4p$ configurations.

Table 3 lists the present BSR results transition probabilities (A_{ji}), oscillator strengths (f_{ij}), and line strengths (S) of the E1 lines for the $3d4s - 3d4p$ transitions in Ti III. The calculated transition probabilities were also used to estimate the lifetimes of the excited levels given in table 1. As another effective assessment of the quality of our target description, our calculated radiative parameters are compared with available experimental data and other theoretical predictions, including the NIST-recommended values [37] as well as oscillator strengths from the WBEPM theory of Zhang *et al* [19], the HFR method of Maati *et al* [22], and the only available experimental measurements of Roberts *et al* [11]. We note overall excellent agreement between our calculations and the NIST-recommended values, showing an average deviation of $\approx 7\%$. Satisfactory agreement is also achieved with the predictions based on the WBEPM and HFR models. The WBEPM theory treats the multi-electron system as a quasi-one-electron problem to simplify the calculation. It appears to slightly underestimate the f-values in most cases listed in the table. The most recent calculations based on the HFR model, which employed the Cowan code [39] with Breit-Pauli corrections, also show good agreement with the present work.

The overall agreement between the results from the different calculations is reasonable, even though some correlation and core-polarization effects in the present structure calculation were omitted due to the use of cut-off parameters as discussed in section 2.1. Larger differences, up to a factor of 2.2, are found when comparing the theoretical predictions with the only available experimental data. According to Roberts *et al*, however, the measured gf-value scale was such a sensitive function of temperature that an uncertainty in the temperature of approximately 5% would result in an uncertainty of about 2 in the value. Consequently, this sensitivity introduced an uncertainty exceeding 50% in the measurements, and additional experiments would be needed to establish a better absolute scale for the Ti III transitions.

Figure 1 displays an extended comparison of the present oscillator strengths (f-values) with the NIST-recommended values [37] for 190 individual E1 transitions involving the targets included in the present BSR-138 model of Ti III. It shows satisfactory agreement between the present calculations and the NIST values, with an average deviation of $\approx 35\%$.

The long lifetimes of the 13 low-lying metastable levels of $3d^2$ and $3d4s$ configurations in Ti III make the forbidden lines good candidates for density and temperature diagnostics of a variety of astrophysical plasmas by straightforward line-intensity ratio measurements. In tables 4 and 5, we present our results for the transition probabilities, oscillator strengths, and line strengths for the dipole-forbidden M1 and E2 lines of the $3d^2 - 3d^2$ and $3d^2 - 3d4s$ transitions. Figure 2 exhibits a comparison of the present f-values with the available NIST-recommended values [37] for 54 M1 and E2 transitions. Excellent agreement is found, even though the magnitudes of the f-values are extremely small for these weak transitions.

The above comparisons of our calculated level energies and radiative parameters with the available experimental data and other theoretical values validate the accuracy of the target wave functions employed in the present work. Our wave functions accurately reproduce the strong E1 transitions in Ti III as well as the weaker M1 and E2 transitions. Recall that the size of our CI expansions for the target states had to be restricted to maintain the computational feasibility of the subsequent scattering calculations. Further improvements in the accuracy of the radiative parameters would require the inclusion of significantly larger configuration expansions. This could be done if only structure results were required.

Table 3. Transition probabilities A_{ji}, oscillator strengths f_{ij}, and line strengths(S) of electric dipole (E1) lines for $3d4s - 3d4p$ transitions in Ti III.

Transition			$A_{ji}(s^{-1})$		f_{ij}					S	
i	j	λ (nm)	Present	NIST [37]	Present	NIST [37]	WBEPM [19]	HFR [22]	Expt. [11]	Present	NIST [37]
10	14	269.296	2.50×10^{6}		4.36×10^{-3}					1.14×10^{-1}	
10	15	256.833	2.71×10^{8}	2.30×10^{8}	2.63×10^{-1}	2.30×10^{-1}	2.33×10^{-1}	9.30×10^{-2}	4.71×10^{-1}	6.60×10^{00}	5.80×10^{00}
10	16	255.734	2.24×10^{7}		3.57×10^{-2}					8.93×10^{-1}	
10	18	254.081	3.32×10^{8}		5.20×10^{-1}		4.40×10^{-1}		8.77×10^{-1}	1.28×10^{1}	
10	21	233.206	4.52×10^{8}	4.30×10^{8}	1.16×10^{-1}	1.20×10^{-1}	1.14×10^{-1}	1.16×10^{-1}		2.59×10^{00}	2.70×10^{00}
10	22	233.237	1.22×10^{8}	1.20×10^{8}	9.35×10^{-2}	9.80×10^{-2}	8.56×10^{-2}	9.37×10^{-2}		2.09×10^{00}	2.30×10^{00}
10	23	232.774	5.30×10^{6}		6.76×10^{-3}		5.72×10^{-3}			1.51×10^{-1}	
11	14	270.276	1.02×10^{7}		1.07×10^{-2}					4.67×10^{-1}	
11	15	257.723	9.72×10^{7}	9.20×10^{7}	5.70×10^{-2}	5.50×10^{-2}		5.58×10^{-2}	1.29×10^{-1}	2.39×10^{00}	2.30×10^{00}
11	16	256.618	2.76×10^{8}		2.67×10^{-1}				5.76×10^{-1}	1.11×10^{1}	
11	17	254.936	7.61×10^{6}		1.02×10^{-2}					4.21×10^{-1}	
11	18	254.953	1.97×10^{7}		1.86×10^{-2}					7.70×10^{-1}	
11	19	252.861	3.57×10^{8}		4.65×10^{-1}					1.91×10^{1}	
11	22	233.972	3.26×10^{8}	3.00×10^{8}	1.51×10^{-1}	1.50×10^{-1}				5.66×10^{00}	5.70×10^{00}
11	23	233.506	7.40×10^{7}	7.70×10^{7}	5.70×10^{-2}	6.30×10^{-2}		5.74×10^{-2}		2.12×10^{00}	2.40×10^{00}
11	24	222.628	1.53×10^{6}		1.59×10^{-3}					5.79×10^{-2}	
11	25	219.308	9.44×10^{5}		3.87×10^{-4}					1.36×10^{-2}	
12	14	271.944	9.30×10^{1}		7.09×10^{-8}					4.36×10^{-6}	
12	16	258.122	6.43×10^{7}		4.50×10^{-2}					2.65×10^{00}	
12	17	256.420	3.63×10^{8}		3.50×10^{-1}				6.09×10^{-1}	2.05×10^{1}	
12	19	254.321	5.46×10^{6}		5.14×10^{-3}		3.50×10^{-2}			2.97×10^{-1}	
12	20	251.682	3.68×10^{8}	3.40×10^{8}	4.36×10^{-1}	4.20×10^{-1}	4.10×10^{-1}	4.43×10^{-1}	6.84×10^{-1}	2.49×10^{1}	2.40×10^{1}
12	23	234.750	3.63×10^{8}	3.30×10^{8}	2.02×10^{-1}	1.90×10^{-1}	2.05×10^{-1}			1.06×10^{1}	1.10×10^{1}
12	24	223.759	7.17×10^{5}		5.35×10^{-4}					2.75×10^{-2}	
13	14	298.561	2.40×10^{8}	1.90×10^{8}	2.99×10^{-1}	2.50×10^{-1}		2.88×10^{-1}	5.51×10^{-1}	1.42×10^{1}	1.20×10^{1}
13	16	281.983	5.29×10^{6}		6.00×10^{-3}					2.72×10^{-1}	
13	17	279.954	2.02×10^{5}		3.17×10^{-4}					1.42×10^{-2}	
13	18	279.974	5.34×10^{6}		5.92×10^{-3}					2.65×10^{-1}	
13	19	277.453	9.94×10^{5}		1.52×10^{-3}					6.72×10^{-2}	
13	22	254.875	7.14×10^{5}		3.82×10^{-4}					1.54×10^{-2}	
13	24	241.472	4.17×10^{8}	3.80×10^{8}	4.95×10^{-1}	4.70×10^{-1}		5.10×10^{-1}		1.94×10^{1}	1.80×10^{1}
13	25	237.572	4.45×10^{8}	4.00×10^{8}	2.09×10^{-1}	2.00×10^{-1}		1.99×10^{-1}		7.84×10^{00}	7.90×10^{00}

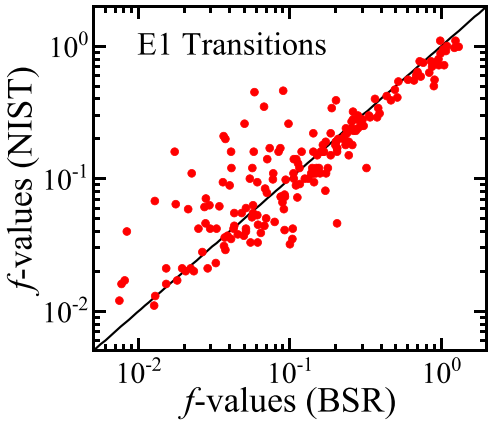

Figure 1. Comparison between the present calculated oscillator strengths (f-values) and the NIST-recommended values [37] for dipole-allowed (E1) transitions in Ti III.

Table 4. Transition probabilities A_{ji}, oscillator strengths f_{ij}, and line strengths(S) of magnetic dipole (M1) lines for $3d^2 - 3d^2$ and $3d^2 - 3d4s$ transitions in Ti III.

i	j	λ (nm)	$A_{ji}(s^{-1})$	f_{ij}	S
1	2	54 083.288	2.26×10^{-4}	1.12×10^{-8}	6.69×10^{00}
1	4	1180.150	6.85×10^{-3}	1.38×10^{-10}	1.99×10^{-3}
1	6	943.076	5.64×10^{-6}	3.80×10^{-14}	4.07×10^{-7}
1	7	932.731	8.34×10^{-6}	9.15×10^{-14}	9.67×10^{-7}
1	10	262.713	7.95×10^{-6}	5.10×10^{-15}	1.68×10^{-8}
1	11	261.787	1.64×10^{-5}	1.74×10^{-14}	5.71×10^{-8}
1	12	260.241	1.12×10^{-6}	1.63×10^{-15}	5.33×10^{-9}
1	13	239.784	2.28×10^{-4}	2.07×10^{-13}	6.29×10^{-7}
2	3	42 462.845	3.86×10^{-4}	1.05×10^{-8}	6.78×10^{00}
2	4	1206.476	1.27×10^{-2}	1.92×10^{-10}	3.96×10^{-3}
2	7	949.100	7.12×10^{-5}	5.78×10^{-13}	8.71×10^{-6}
2	8	703.596	5.75×10^{-3}	4.96×10^{-11}	5.74×10^{-4}
2	11	263.061	2.19×10^{-6}	1.67×10^{-15}	7.75×10^{-9}
2	12	261.499	6.82×10^{-6}	7.20×10^{-15}	3.31×10^{-8}
2	13	240.851	4.64×10^{-4}	3.03×10^{-13}	1.30×10^{-6}
3	8	715.451	9.08×10^{-3}	6.31×10^{-11}	9.57×10^{-4}
3	12	263.119	8.59×10^{-6}	7.16×10^{-15}	4.26×10^{-8}
4	6	4694.615	2.29×10^{-3}	2.40×10^{-10}	1.01×10^{-2}
4	7	4448.992	4.75×10^{-3}	7.51×10^{-10}	3.02×10^{-2}
4	10	337.942	1.55×10^{-4}	1.68×10^{-13}	7.20×10^{-7}
4	11	336.412	1.70×10^{-5}	3.02×10^{-14}	1.29×10^{-7}
4	12	333.862	7.29×10^{-5}	1.79×10^{-13}	7.55×10^{-7}
4	13	300.926	1.60×10^{-6}	2.34×10^{-15}	9.01×10^{-9}
5	6	153 374.233	6.32×10^{-6}	5.73×10^{-9}	2.01×10^{00}
6	7	85 034.014	4.04×10^{-5}	4.86×10^{-9}	2.50×10^{00}
6	9	457.208	1.17×10^{-1}	1.28×10^{-10}	4.44×10^{-4}
6	10	364.156	8.21×10^{-6}	1.83×10^{-14}	5.25×10^{-8}
6	11	362.380	4.96×10^{-7}	1.82×10^{-15}	5.19×10^{-9}
6	13	321.536	1.08×10^{-4}	3.18×10^{-13}	8.12×10^{-7}
7	11	363.931	1.67×10^{-6}	3.73×10^{-15}	1.78×10^{-8}
7	12	360.948	2.79×10^{-6}	8.54×10^{-15}	4.03×10^{-8}
7	13	322.757	3.25×10^{-4}	5.80×10^{-13}	2.48×10^{-6}
8	12	416.174	1.62×10^{-10}	3.66×10^{-19}	3.59×10^{-12}

Table 5. Transition probabilities A_{ji}, oscillator strengths f_{ij}, and line strengths(S) of electric quadrupole (E2) lines for $3d^2 - 3d^2$ and $3d^2 - 3d4s$ transitions in Ti III.

i	j	λ (nm)	$A_{ji}(s^{-1})$	f_{ij}	S
1	2	54 083.288	2.56×10^{-12}	1.26×10^{-16}	4.30×10^{-1}
1	3	23 786.870	5.78×10^{-12}	6.97×10^{-17}	1.96×10^{-2}
1	4	1180.150	1.35×10^{-5}	2.73×10^{-13}	1.27×10^{-2}
1	5	948.911	6.49×10^{-2}	1.48×10^{-10}	2.91×10^{00}
1	6	943.076	2.23×10^{-2}	1.50×10^{-10}	2.91×10^{00}
1	7	932.731	2.02×10^{-3}	2.21×10^{-11}	4.12×10^{-1}
1	8	694.560	2.64×10^{-5}	3.10×10^{-13}	2.65×10^{-3}
1	9	307.924	7.13×10^{-3}	1.97×10^{-12}	1.65×10^{-3}
1	10	262.713	3.73×10^{1}	2.39×10^{-8}	1.35×10^{1}
1	11	261.787	1.63×10^{1}	1.73×10^{-8}	9.66×10^{00}
1	12	260.241	1.20×10^{00}	1.75×10^{-9}	9.58×10^{-1}
1	13	239.784	2.17×10^{-2}	1.97×10^{-11}	8.74×10^{-3}
2	3	42 462.845	7.50×10^{-12}	2.03×10^{-16}	4.46×10^{-1}
2	4	1206.476	8.99×10^{-6}	1.36×10^{-13}	9.54×10^{-3}
2	6	959.813	4.07×10^{-2}	2.03×10^{-10}	5.81×10^{00}
2	7	949.100	1.31×10^{-2}	1.06×10^{-10}	2.91×10^{00}
2	8	703.596	1.68×10^{-6}	1.45×10^{-14}	1.81×10^{-4}
2	10	263.995	1.82×10^{1}	8.44×10^{-9}	6.81×10^{00}
2	11	263.061	2.77×10^{1}	2.12×10^{-8}	1.69×10^{1}
2	12	261.499	1.23×10^{1}	1.30×10^{-8}	1.01×10^{1}
2	13	240.851	1.74×10^{-1}	1.14×10^{-10}	7.17×10^{-2}
3	4	1241.758	4.25×10^{-5}	5.33×10^{-13}	5.29×10^{-2}
3	7	970.798	4.45×10^{-2}	2.94×10^{-10}	1.12×10^{1}
3	8	715.451	1.74×10^{-5}	1.21×10^{-13}	2.05×10^{-3}
3	11	264.700	1.16×10^{1}	6.97×10^{-9}	7.30×10^{00}
3	12	263.119	4.26×10^{1}	3.55×10^{-8}	3.64×10^{1}
3	13	242.225	3.48×10^{-2}	1.80×10^{-11}	1.48×10^{-2}
4	5	4842.850	2.23×10^{-7}	8.17×10^{-15}	1.04×10^{-2}
4	6	4694.615	3.23×10^{-7}	3.38×10^{-14}	3.99×10^{-2}
4	7	4448.992	1.85×10^{-10}	2.92×10^{-17}	2.98×10^{-5}
4	8	1688.020	5.42×10^{-4}	3.42×10^{-11}	3.63×10^{00}
4	9	416.632	7.16×10^{00}	3.63×10^{-9}	7.53×10^{00}
4	10	337.942	2.69×10^{-2}	2.91×10^{-11}	3.61×10^{-2}
4	11	336.412	8.78×10^{-2}	1.57×10^{-10}	1.91×10^{-1}
4	12	333.862	2.30×10^{-2}	5.63×10^{-11}	6.69×10^{-2}
4	13	300.926	1.77×10^{1}	2.58×10^{-8}	2.34×10^{1}
5	7	54 704.595	2.80×10^{-11}	4.55×10^{-15}	2.75×10^{00}
5	11	361.526	1.39×10^{00}	1.52×10^{-8}	5.08×10^{00}
5	13	320.864	6.64×10^{-3}	5.85×10^{-11}	1.40×10^{-2}
6	7	85 034.014	8.58×10^{-12}	1.03×10^{-15}	6.17×10^{00}
6	10	364.156	3.01×10^{00}	6.73×10^{-9}	6.91×10^{00}
6	11	362.380	3.42×10^{-1}	1.26×10^{-9}	1.27×10^{00}
6	12	359.423	1.44×10^{00}	7.26×10^{-9}	7.11×10^{00}
6	13	321.536	2.57×10^{-3}	7.59×10^{-12}	5.50×10^{-3}
7	8	2720.052	1.39×10^{-7}	3.13×10^{-14}	2.24×10^{-2}
7	9	459.679	1.93×10^{-2}	1.28×10^{-11}	3.99×10^{-2}
7	10	365.722	9.69×10^{-1}	1.31×10^{-9}	2.29×10^{00}
7	11	363.931	2.30×10^{00}	5.13×10^{-9}	8.77×10^{00}
7	12	360.948	2.80×10^{00}	8.56×10^{-9}	1.42×10^{1}
7	13	322.757	1.18×10^{-1}	2.11×10^{-10}	2.59×10^{-1}
8	11	420.144	2.75×10^{-2}	4.53×10^{-11}	2.15×10^{-1}
8	12	416.174	3.90×10^{-4}	8.80×10^{-13}	4.02×10^{-3}
8	13	366.211	1.21×10^{1}	1.55×10^{-8}	5.02×10^{1}
9	13	1083.568	3.77×10^{-3}	4.73×10^{-10}	6.11×10^{00}

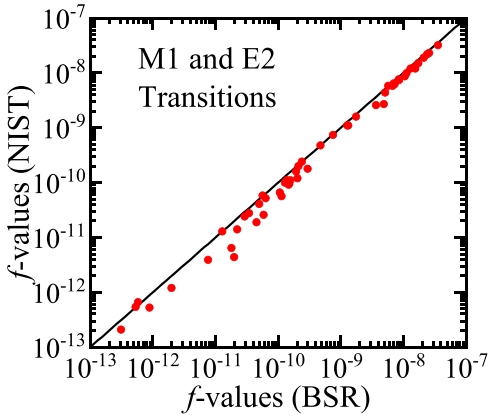

Figure 2. Comparison between the present calculated oscillator strengths (f-values) and the NIST-recommended values [37] for forbidden M1 and E2 transitions in Ti III.

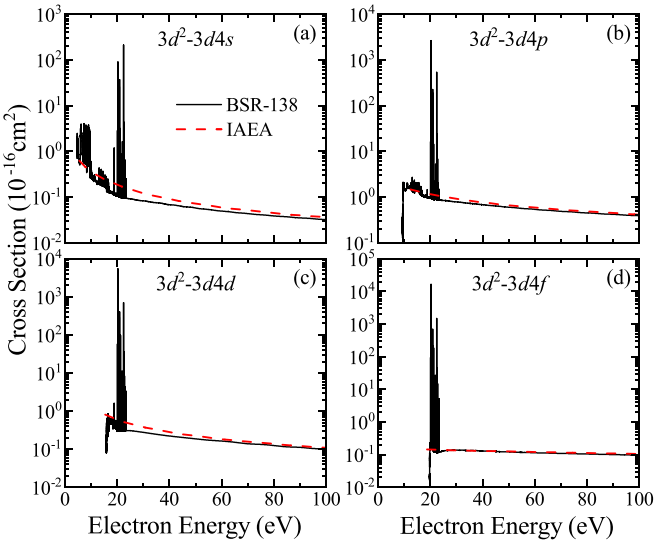

Figure 3. Cross sections for electron impact excitation from the $3d^2$ $^3F_2$ ground state to the excited $3d4s$, $3d4p$, $3d4d$, and $3d4f$ configurations of Ti III. The solid (black) line represents the present work, while the dashed (red) line corresponds to available results from the IAEA ALADDIN database [24].

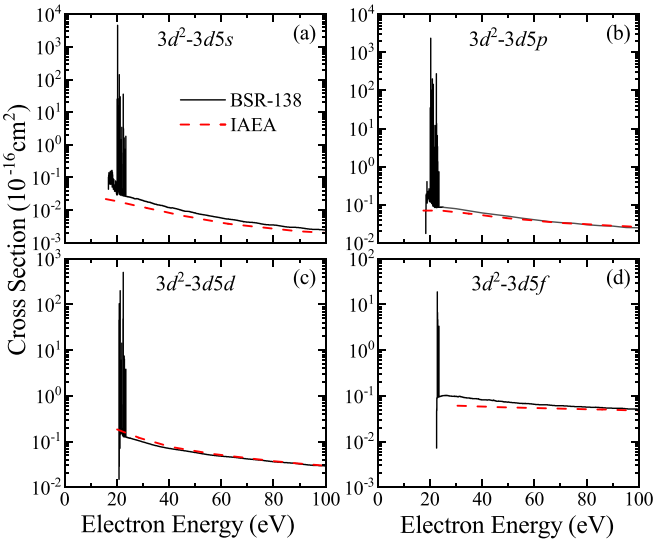

Figure 4. Cross sections for electron impact excitation from the $3d^2$ $^3F_2$ ground state to the excited $3d5s$, $3d5p$, $3d5d$, and $3d5f$ configurations of Ti III. The solid (black) line represents the present work, while the dashed (red) line corresponds to available results on the IAEA ALADDIN database [24].

3.2. Collisional Parameters

In this section, we present our calculated electron-collisional parameters including excitation cross Sections and effective collision strengths for selected forbidden and allowed transitions in Ti III. We repeat that systematic investigations regarding electron impact excitation of Ti III are extremely scarce. The only available data for comparison were taken from the IAEA ALADDIN database [24] for the valence electron excited to higher orbitals rather than fine-structure-resolved levels.

Figures 3–5 present our calculated cross sections for single-electron excitations from the $3d^2$ $^3F_2$ ground state to the excited $3d4l$ ($l=0-3$), $3d5l$ ($l=0-3$), and $3d6l$ ($l=0,1$) configurations, respectively, in comparison with the cross sections collected from the IAEA ALADDIN database [24]. To ensure that the comparisons are meaningful, the BSR-138 curves shown in the figures were obtained by summing all excitation cross sections from the ground level $3d^2$ $^3F_2$ to the corresponding excited $3dnl$ configurations. Overall excellent agreement is found between the present BSR-138 calculations and the IAEA data, both in the magnitude and the energy dependence of the curves. The comparisons validate the accuracy of the present collision calculations using the BSR-138 model.

Figure 6 shows the present BSR-138 results for the cross sections as a function of the incident electron energy (in eV) and the corresponding Maxwellian-averaged effective collision strengths as a function of the electron temperature (in K) for the fine-structure-resolved transitions between the ground

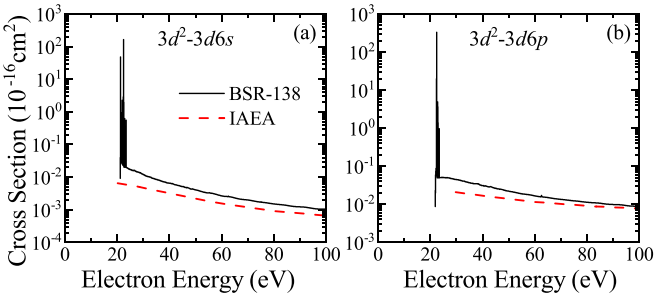

Figure 5. Cross sections for electron impact excitation from the $3d^2\ ^3F_2$ ground state to the excited $3d6s$ and $3d6p$ configurations of Ti III. The solid (black) line represents the present work, while the dashed (red) line corresponds to available results from the IAEA ALADDIN database [24].

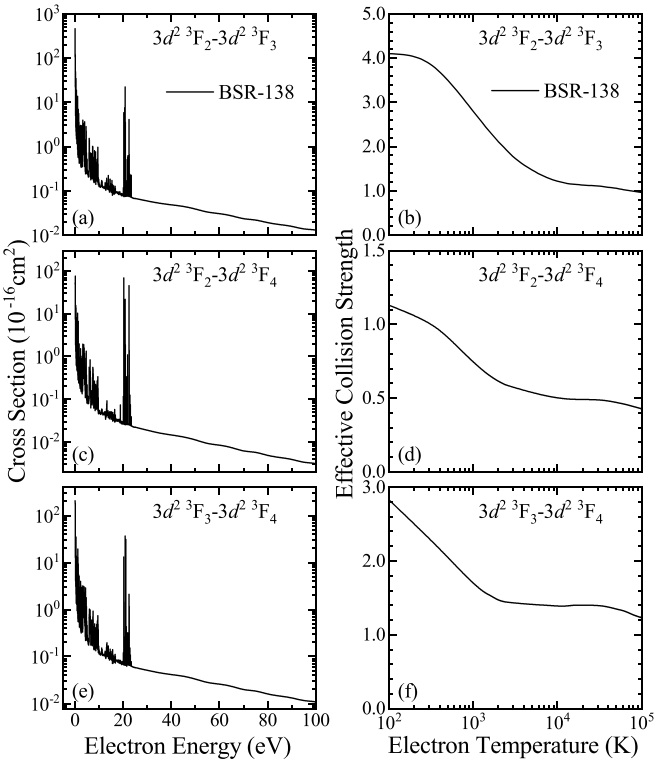

Figure 6. Electon impact excitation cross sections and effective collision strengths for the fine-structure-forbidden transitions (a), (b) $3d^2\ ^3F_2 - 3d^2\ ^3F_3$, (c), (d) $3d^2\ ^3F_2 - 3d^2\ ^3F_4$, and (e), (f) $3d^2\ ^3F_3 - 3d^2\ ^3F_4$ in Ti III.

state $^3F_2$ and the metastable states $^3F_3$, $^3F_4$ of the ground $3d^2$ configuration. Panels (a), (c), and (e) show pronounced resonance structures in the energy dependence of the cross sections in the low-energy region up to 25 eV. These resonant features significantly exceed the background values and play a pivotal role in determining the thermally averaged collision strengths at low temperatures. Such behavior is a characteristic feature of forbidden transitions observed in electron-ion collision processes. These resonance structures arise from Rydberg series of narrow resonances converging to various excitation thresholds. They are associated with the temporary capture of the scattered electron into highly-excited nl orbitals of the target, owing to the strong attractive Coulomb force from the doubly-charged Ti III ion.

The corresponding effective collision strengths for these forbidden transitions, displayed in figures 6(b), (d) and (f), exhibit distinct characteristics as the electron temperature increases. At low temperatures, the effective collision strengths are significantly enhanced due to the resonance structures in the cross sections. However, as the temperature rises, the curves show a decreasing trend, reflecting the diminishing influence of resonances relative to the non-resonant background contributions. The effective collision strengths converge to a non-zero asymptotic value when the electron temperature approaches 10^4 K. Furthermore, the relative magnitudes of the effective collision strengths for different transitions can vary significantly, reflecting the transition probabilities and coupling strengths between the initial and final states. For instance, the $^3F_2 - {}^3F_3$ transition has a consistently higher effective collision strength compared to the $^3F_2 - {}^3F_4$ transition across the entire temperature range. This suggests a stronger coupling for the transition with $\Delta J = 1$, since the transition with $\Delta J = 2$ requires a higher multipole interaction than $\Delta J = 1$.

Figure 7 displays our predicted cross sections and effective collision strengths for the fine-structure-forbidden transitions from the ground state $3d^2\ ^3F_2$ to the $^3D_1$, $^3D_2$, $^3D_3$, and $^1D_2$ of the first excited configuration $3d4s$. The cross sections exhibit a similarly strong resonance structures in the low-energy region as seen in figure 6. However, the corresponding effective collision strengths exhibit different trends at higher electron temperatures above 10^4 K. All curves have a maximum at temperatures between 10^4 K and 10^5 K.

This can be explained by considering the nature of equation (4), where the exponential term controls how much of the collision strength contributes when performing the integration. This exponential term depends on the electron temperature T_e, which results in a flatter exponential curve at higher temperature. Therefore, the larger effective collision strengths at lower temperatures in the present calculations is due to the enhanced resonance structure in the near-threshold region. The contributions from the higher energy resonances become significant when the electron temperature rises. For the $3d^2$ transitions shown in figures 6(a)–(e), the magnitudes of the near-threshold resonances at low energies are relatively larger than those at energies close to 25 eV, thus leading to flatter curves in figures 6(b), (d) and (f) at high temperature. For the $3d^2 - 3d4s$ transitions displayed in figure 7, the resonances at energies close to 25 eV are one order of magnitude larger than at low energy, which results in the rising of the effective collision-strength curves at temperatures between 10^4 K and 10^5 K. Especially for the $3d^2\ ^3F_2 - 3d4s\ ^1D_2$ transition, the apparent flatness of the effective collision strengths at low temperatures occurs due to the smaller magnitude of the resonances seen in figure 7(g) at low impact energy.

The BSR-138 results for optically allowed transitions related to selected ultraviolet lines, 241.472 nm, 251.682 nm, 256.420 nm, and 298.561 nm, are shown in figures 8 and 9. These lines were observed with relatively large intensity in the

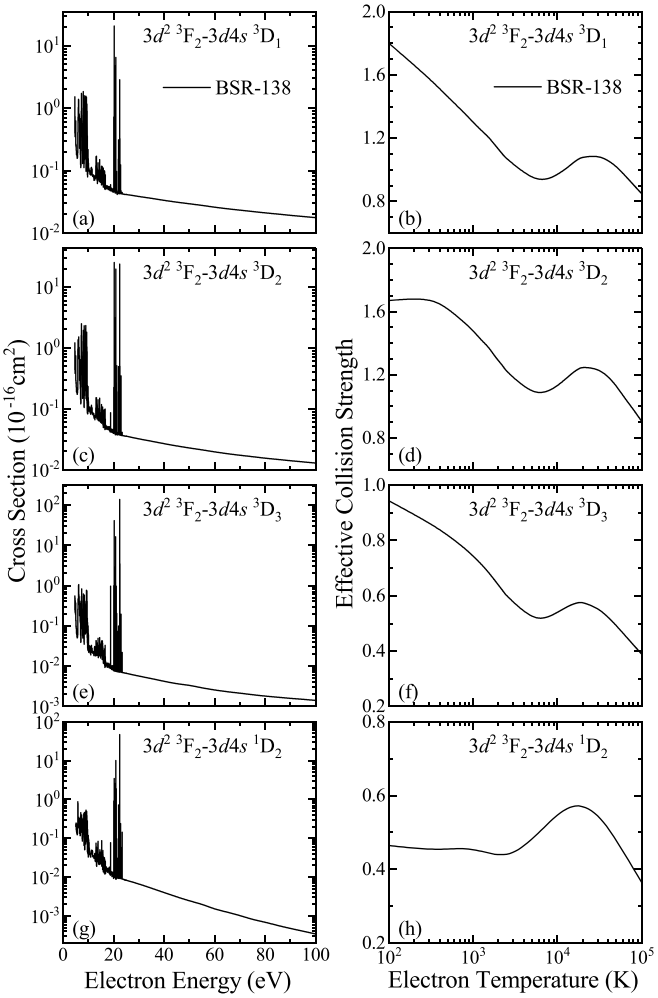

Figure 7. Electon impact excitation cross sections and effective collision strengths for the fine-structure-forbidden transitions (a), (b) $3d^2\ ^3F_2 - 3d4s\ ^3D_1$, (c), (d) $3d^2\ ^3F_2 - 3d4s\ ^3D_2$, (e), (f) $3d^2\ ^3F_2 - 3d4s\ ^3D_3$, and (g), (h) $3d^2\ ^3F_2 - 3d4s\ ^1D_2$ in Ti III.

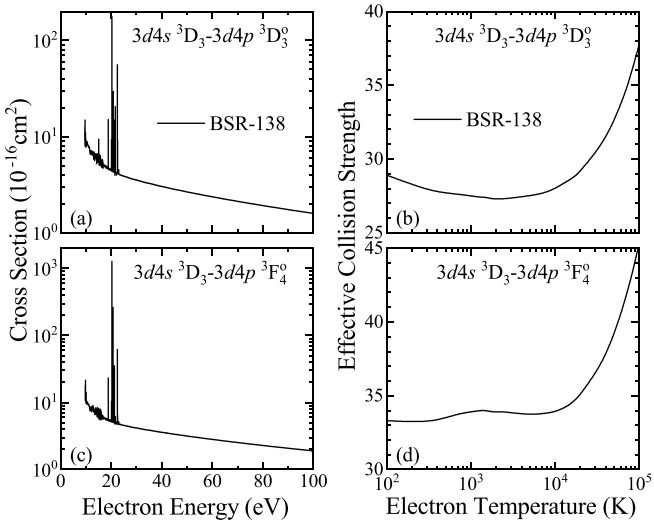

Figure 8. Electon impact excitation cross sections and effective collision strengths for the fine-structure-allowed transitions (a), (b) $3d4s\ ^3D_3 - 3d4p\ ^3D^o_3$ and (c), (d) $3d4s\ ^3D_3 - 3d4p\ ^3F^o_4$ in Ti III.

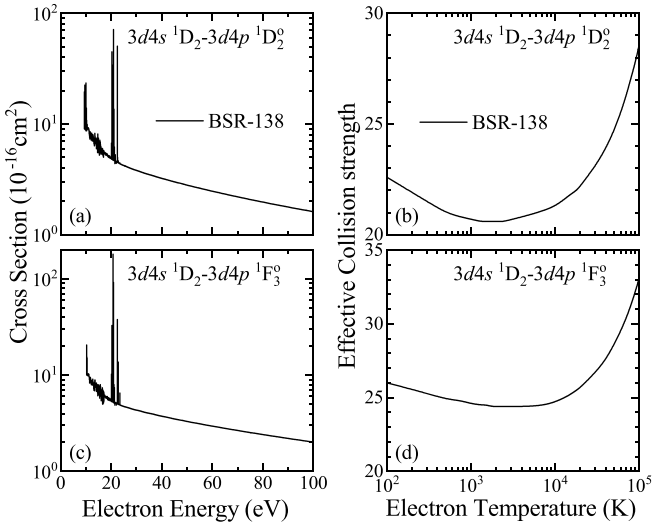

Figure 9. Electon impact excitation cross sections and effective collision strengths for the fine-structure-allowed transitions (a), (b) $3d4s\ ^1D_2 - 3d4p\ ^1D^o_2$, (c), (d) $3d4s\ ^1D_2 - 3d4p\ ^1F^o_3$ of Ti III.

experimental spectra detected from the main products of cathodic ionization in the micro-cathode arc thruster μCAT [6]. Figure 8 exhibits the results for transitions from $3d4s\ ^3D_3$ to $3d4p\ ^3D^o_3$ and $^3F^o_4$ corresponding to the 256.420 nm and 251.682 nm lines, respectively, while Figure 9 shows the results for transitions from $3d4s\ ^1D_2$ to $3d4p\ ^1D^o_2$ and $^1F^o_3$ corresponding to the 298.561 nm and 241.472 nm lines.

The curves of the present BSR-138 calculations behave similarly for these cases, which are characteristic for optically allowed transitions. Recall that the magnitude of the cross sections at higher energies is directly related to the corresponding electric dipole oscillator strength. The latter values are generally larger than 0.1 (cf table 3) and are indeed among the highest group in the table. Consequently, the cross sections for these transitions are generally two or even three orders of magnitude larger than those for the forbidden transitions shown in figures 6 and 7 in the non-resonant background, thereby leading to overall large effective collision strengths. The near-threshold resonance structures are relatively less pronounced and smaller, thus resulting in flatter curves of the effective collision strengths at low temperatures. The curves start to rise rapidly at temperatures above 10^4 K mainly due to the large non-resonant background. The large resonances at high energies could also raise the curves of effective collision strength, which might be observed by comparing panels (b) and (d) of figure 8.

The calculated electron collision and radiative parameters are useful for the modeling and diagnostics of Ti plasmas. They can be employed for solving the population balance equations of the related CR model or generating line intensities using a spectral synthesis code such as CLOUDY [40]. The spectral lines of Ti ions were detected by Ji *et al* [6,

7] to explore the influence of energy-supply modes with different discharge characteristics on the microphysical process in the plasma propulsion device μCAT. The Ti II spectrum at wavelengths near 330 nm and the Ti III spectrum at wavelengths near 250 nm were identified. Their results showed a significant difference in the proportion between the spectral radiation intensities of Ti II and Ti III generated by the ionization of cathode metal under different energy-supply modes. Accurate atomic data for a large number of dipole-allowed and forbidden transitions are hence of primary importance for the development of a reliable CR model for such processes.

4. Summary

We performed a detailed theoretical investigation of the electron-impact excitation of doubly-ionized titanium (Ti III) using the sophisticated *B*-spline *R*-matrix (BSR) method. Extensive results where obtained for radiative parameters as well as excitation cross sections and effective collision strengths for all forbidden and optically allowed transitions between the 138 fine-structure levels of Ti III belonging to the $3d^2$, $4s^2$, $4s4p$, $3d4l$ ($l=0-3$), $3d5l$ ($l=0-3$), $3d6s$, and $3d6p$ configurations. To our knowledge, the comprehensive data sets provided in this work are the only systematic and consistent results for electron-impact excitation of the Ti III fine-structure levels, thereby enabling a detailed analysis of the observed spectral lines of titanium and its applications in plasma modeling and diagnostics.

The BSR codes employed in this work were considerably modified and extended to handle the complex open $3d$ sub-shell of iron-peak elements. The method is based on the close-coupling *R*-matrix theory, using *B*-splines as the basis for representing the continuum wavefunctions. Utilizing non-orthogonal orbital sets, both for the construction of the target wave functions and the representation of the scattering functions, allowed us to optimize the individual wave functions independently, and hence to generate a more accurate description of the target than what is usually possible with orthogonal orbital sets. This is essential if the target states are to be used in a subsequent collision calculation. The important configurations were carefully chosen in the CI expansions to account as much as possible for relaxation, valence-valence, and core-valence correlation effects. Furthermore, relativistic effects were included in the close-coupling expansions through one-electron terms of the Breit-Pauli Hamiltonian.

The calculated excitation energies and radiative parameters show good agreement with the available values from the NIST database and previous work reported in the literature. Our target-state wave functions accurately reproduce the strong E1 transitions as well as the weaker M1 and E2 transitions in Ti III. Finally, the accuracy of the present calculated excitation cross sections has been validated, also by comparison with the results available from the IAEA ALADDIN database. The complete list of radiative and collisional data generated in this study is available from the authors upon request.

Data availability statement

All data that support the findings of this study are included within the article (and any supplementary files).

Acknowledgments

This work was supported by the Fundamental Research Funds for the Central Universities No. 2023FRFK06006 and the National Natural Science Foundation of China under Grant No. U22B2094. The work of K B was supported by the United States National Science Foundation under Grant No. PHY-2110023.

Ethical compliance

All procedures performed in studies involving human participants were in accordance with the ethical standards of the institutional and/or national research committee and with the 1964 Helsinki Declaration and its later amendments or comparable ethical standards.

Conflict of interest

The authors declare that they have NO affiliations with or involvement in any organization or entity with any financial interest in the subject matter or materials discussed in this manuscript.

ORCID iDs

Yang Wang https://orcid.org/0000-0002-5655-3830
Qiu-Yao Cao https://orcid.org/0009-0005-5650-4448
Xi-Ming Zhu https://orcid.org/0000-0002-6501-0096
Chun-Meng Du https://orcid.org/0009-0007-9847-9337
Klaus Bartschat https://orcid.org/0000-0001-6215-5014

References

[1] Karabadzhak G F, Chiu Y h and Dressler R A 2006 *J. Appl. Phys.* **99** 113305
[2] Dressler R A, Chiu Y h, Zatsarinny O, Bartschat K, Srivastava R and Sharma L 2009 *J. Phys. D: Appl. Phys.* **42** 185203
[3] Zhu X M, Wang Y F, Wang Y, Yu D R, Zatsarinny O, Bartschat K, Tsankov T V and Czarnetzki U 2019 *Plasma Sources Sci. Technol.* **28** 105005
[4] Priti, Gangwar R K and Srivastava R 2019 *Plasma Sources Sci. Technol.* **28** 025003
[5] Baghel S S, Priti and Srivastava R 2023 *Plasma Sources Sci. Technol.* **32** 065020
[6] Ji T, Wei L, Wang L, Zhao Y, Li T, Liang T, Li H, Zhu X and Ding Y 2023 *J. Phys. D. Appl. Phys.* **56** 245201
[7] Ji T, Wei L, Wang L, Li J, Zhao Y, Ren Z, Liang T, Ma H, Li H and Zhu X 2023 *J. Appl. Phys.* **134** 033304
[8] Meier S M, Hecimovic A, Tsankov T V, Luggenhölscher D and Czarnetzki U 2018 *Plasma Sources Sci. Technol.* **27** 035006
[9] Roberts J, Andersen T and Sørensen G 1973 *Nucl. Instrum. Meth.* **110** 119

[10] Andersen T, Petersen P and Biemont E 1977 *J. Quant. Spectrosc. Radiat. Transf.* **17** 389
[11] Roberts J, Voigt P and Czernichowski A 1975 *Astrophys. J.* **197** 791–8
[12] Baudinet-Robinet Y, Dumont P, Garnir H, Grevesse N and Biemont E 1980 *J. Opt. Soc. Am.* **70** 464–6
[13] Warner B and Kirkpatrick R C 1969 *Mon. Not. R. Astron. Soc.* **144** 397
[14] Biémont E 1976 *J. Quant. Spectrosc. Radiat. Transf.* **16** 137–42
[15] Beck D R 1981 *Phys. Rev.* A **23** 159
[16] Biémont E, Hansen J, Quinet P and Zeippen C 1992 *J. Phys. B: At. Mol. Opt. Phys.* **25** 5029
[17] Raassen A and Uylings P 1997 *Astrophys. J. Suppl. Ser.* **123** 147
[18] Safronova U, Johnson W, Kato D and Ohtani S 2001 *Phys. Rev.* A **63** 032518
[19] Zhang T Y, Zheng N W and Ma D X 2009 *Int. J. Quantum Chem.* **109** 145
[20] El-Maaref A, Samak Z, Allam S and El-Sherbini T M 2015 *Int. J. New. Hor. Phys* **2** 25
[21] Fivet V, Quinet P and Bautista M 2016 *Astron. Astrophys.* **585** A121
[22] El Maati L A, Mahmoudi W F, Alkallas F, Nessib N B and Dimitrijević M S 2023 *Adv. Space Res.* **71** 1307
[23] Popović D, Bannister M, Clark R, Chung Y S, Djurić N, Meyer F, Müller A, Neau A, Pindzola M and Smith A 2002 *Phys. Rev.* A **65** 034704
[24] Clark R and Abdallah J J 2003 IAEA-APID-11 (available at: www-amdis.iaea.org/ALADDIN/collision.html)
[25] Zatsarinny O 2006 *Comput. Phys. Commun.* **174** 273
[26] Zatsarinny O and Bartschat K 2008 *Phys. Rev.* A **77** 062701
[27] Zatsarinny O and Bartschat K 2013 *J. Phys. B: At. Mol. Opt. Phys.* **46** 112001
[28] Tayal S and Zatsarinny O 2018 *Phys. Rev.* A **98** 012706
[29] Tayal S and Zatsarinny O 2020 *Astrophys. J.* **888** 10
[30] Tayal S and Zatsarinny O 2020 *Astrophys. J.* **905** 101
[31] Tayal S and Zatsarinny O 2022 *Astrophys. J. Suppl. Ser.* **259** 52
[32] Zatsarinny O and Fischer C F 2009 *Comp. Phys. Commun.* **180** 2041
[33] Fischer C F, Tachiev G, Gaigalas G and Godefroid M R 2007 *Comput. Phys. Commun.* **176** 559
[34] Available at: http://netlib.org/scalapack/
[35] Badnell N 1999 *J. Phys. B: At. Mol. Opt. Phys.* **32** 5583
[36] Seaton M J 1987 *J. Phys. B: At. Mol. Opt. Phys.* **20** 6363
[37] Kramida A, Yu R and Reader J (NIST ASD Team) 2023 NIST atomic spectra database (ver. 5.11) (National Institute of Standards and Technology) (available at: https://physics.nist.gov/asd)
[38] Grünberger S, Watzl G, Huber N, Eschlböck-Fuchs S, Hofstadler J, Pissenberger A, Duchaczek H, Trautner S and Pedarnig J D 2020 *Opt. Laser Techn.* **123** 105944
[39] Cowan R D 1981 *The Theory of Atomic Structure and Spectra* (University of California Press)
[40] Chatzikos M, Bianchi S, Camilloni F, Chakraborty P, Gunasekera C M, Guzmán F, Milby J S, Sarkar A, Shaw G and van Hoof P A 2023 (arXiv: 2308.06396)